AIAA Modeling and Simulation Technologies Conference
10 - 13 August 2009, Chicago, Illinois

AIAA 2009-6236

Trajectory-based Accurate Linearization of the 155mm Spin-stabilized Projectile Dynamics

Spilios THEODOULIS* Yannick MOREL* Philippe WERNERT†

This paper addresses the problem of accurately linearizing the nonlinear dynamics of the 155mm spin-stabilized rigid-body projectile about a given state trajectory using a body-rolling reference frame. Current approaches result in rather simplistic mathematical models, based on restrictive assumptions on the system's state behavior, subsequently used for stability analysis, trajectory prediction and control. These models are not always thorough enough to provide an accurate measure of the system's behavior and may neglect important dynamics crucial for the guidance and control tasks. In this work, the 6DoF projectile dynamics are modeled using a tensor-like formulation and appropriate aerodynamic functions and then systematically linearized about a given time trajectory. The resulting linear, time-varying state space system matrices are computed, and their components validated through comparisons with numerical linearization techniques. The obtained system model is finally used for local stability analysis through frozen-time theory and simplified stability conditions are obtained. Finally a connection with existing classical results from aeroballistics theory is performed so as to validate the presented approach.

Nomenclature

Acronyms

AoA	=	Angle of Attack
AoS	=	Angle of Sideslip
CG	=	Center of Gravity
$\mathrm{CP_f}$	=	Aerodynamic force Center of Pressure
$\mathrm{CP_m}$	=	Magnus force Center of Pressure
LPV	=	Linear Parameter-Varying
LTI	=	Linear Time-Invariant
LTV	=	Linear Time-Varying
MOI	=	Moment of Inertia Tensor

Symbols & Notations

$\mathbf{A}^\top, \mathbf{A}^{-1}$	=	Matrix transpose, matrix inverse
$\overline{\mathscr{C}}_-$	=	Field of closed left-half plane complex numbers
$\mathscr{D}^i$	=	Derivative operator with respect to frame i
$\mathbf{f}\big\vert_{\mathcal{T}}$	=	Vector-valued function $\mathbf{f}$ evaluated along a trajectory $\mathcal{T}$
$\mathscr{R}$	=	Field of real numbers
$\Re, \Im$	=	Real, imaginary part of a complex number
s_x, c_x, t_x	=	Sine, cosine, tangent of variable x
$[\mathbf{T}]^i, [\mathbf{t}]^i$	=	Tensor $\mathbf{T}$, vector $\mathbf{t}$ expressed in the coordinate system i
$[\mathbf{T}]^{ij}$	=	Transformation matrix from coordinate system j to coordinate system i
$\mathbf{x}_0, \mathbf{x}(t_0)$	=	Initial condition for the state vector $\mathbf{x}(t; t_0)$ at $t = t_0$
$x_\mathrm{r}, \hat{x}, x_\delta$	=	Reference, approximation and perturbed value of variable x

*Dr. Eng., Guidance, Navigation & Control Department, French-German Research Institute of Saint-Louis, 5 rue du Général Cassagnou, 68300, Saint-Louis, FRANCE, Spilios.Theodoulis@isl.eu, Yannick.Morel@isl.eu.

†Dr. Eng., Guidance, Navigation & Control Department Head, French-German Research Institute of Saint-Louis, 5 rue du Général Cassagnou, 68300, Saint-Louis, FRANCE, Philippe.Wernert@isl.eu.

$\mathscr{S}$	=	Forced autonomous nonlinear dynamical system
$\hat{\mathscr{S}}$	=	Forced non-autonomous LTV dynamical system
$\hat{\mathscr{S}}_{\mathbf{x}}$	=	Unforced non-autonomous LTV dynamical system
$\nabla_x f$	=	Partial derivative of function f with respect to variable x
$\nabla_{\mathbf{x}}\mathbf{f}$	=	Partial derivative of vector-valued function $\mathbf{f}$ with respect to vector $\mathbf{x}$
$\mathbf{O}_{i\times j}$	=	$i \times j$ - dimensional null matrix
$\lambda_i\{\mathbf{A}\}$	=	Matrix $\mathbf{A}$ i$^{\text{th}}$ eigenvalue

Variables

a	=	Speed of sound, m/s
$\mathbf{A}$	=	State system matrix
$\mathbf{A}_{\mathrm{dd}}, \mathbf{A}_{\mathrm{dk}}$	=	Stability, perturbation matrix
$\mathbf{A}_{\boldsymbol{\omega\omega}}, \mathbf{A}_{\boldsymbol{\omega v}}, \mathbf{A}_{\mathbf{v}\boldsymbol{\omega}}, \mathbf{A}_{\mathbf{vv}}$	=	Stability matrix submatrices
$\mathbf{A}_{\boldsymbol{\omega}\mathbf{E}}, \mathbf{A}_{\boldsymbol{\omega}\mathbf{S}}, \mathbf{A}_{\mathbf{v}\mathbf{E}}, \mathbf{A}_{\mathbf{vS}}$	=	Perturbation matrix submatrices
$\mathbf{B}$	=	Input system matrix
$C_{\mathrm{A}}, C_{\mathrm{D}}, C_{\mathrm{L}\alpha}, C_{\mathrm{N}\alpha}, C_{\mathrm{Y}\beta}$	=	Static force aerodynamic coefficients
$C_{\mathrm{m}\alpha}, C_{\mathrm{n}\beta}$	=	Static moment aerodynamic coefficients
$C_{\mathrm{l}p}, C_{mq}, C_{\mathrm{n}r}$	=	Damping moment aerodynamic coefficients
$C_{yp\alpha}, C_{\mathrm{n}p\alpha}$	=	Magnus force & moment aerodynamic coefficients
d	=	Projectile caliber, m
$\mathbf{e}^{\mathrm{be}}$	=	Euler angle vector
f_i	=	Projectile nonlinear dynamics function components
$\mathbf{f}$	=	Projectile nonlinear dynamics vector-valued function
$\mathbf{F}$	=	External force vector
$\mathbf{F}_{\mathrm{D}}, \mathbf{F}_{\mathrm{L}}, \mathbf{F}_{\mathrm{K}}, \mathbf{F}_{\mathrm{W}}$	=	Drag, lift, Magnus, gravity force vectors
g	=	Gravity acceleration, m/s^2
$\mathbf{I}_{\mathrm{b}}^{\mathrm{b}}$	=	Projectile MOI tensor referred to its CG
m	=	Projectile mass, kg
M	=	Mach number
$\mathbf{M}_{\mathrm{b}}$	=	External moment vector
$\mathbf{M}_{\mathrm{PY}}, \mathbf{M}_{\mathrm{K}}, \mathbf{M}_{\mathrm{Rd}}, \mathbf{M}_{\mathrm{PYd}}$	=	Pitch-yaw, Magnus, damping roll-pitch-yaw moment vectors
p, q, r	=	Roll, pitch, yaw velocities, rad/s
$\overline{q}$	=	Dynamic pressure, Pa
$\mathbf{s}_{\mathrm{be}}$	=	Linear displacement vector
S	=	Projectile reference surface, m^2
$S_{\mathrm{d}}, S_{\mathrm{g}}$	=	Dynamic, gyroscopic stability coefficients
u, v, w	=	Longitudinal, lateral, normal velocities, m/s
$\mathbf{u}$	=	Input vector
$\mathbf{v}_{\mathrm{b}}^{\mathrm{e}}$	=	Projectile body frame linear velocity vector wrt to earth frame
V	=	Airspeed, m/s
$x_{\mathrm{e}}, y_{\mathrm{e}}, z_{\mathrm{e}}$	=	Horizontal, lateral, vertical displacements, m
$\mathbf{x}, \mathbf{x}_{\mathrm{d}}, \mathbf{x}_{\mathrm{k}}$	=	State vector, dynamics state vector, kinematics state vector
$\mathbf{w}$	=	Perturbation vector
α	=	Angle of attack, rad
α_{t}	=	Aeroballistic incidence angle, rad
β	=	Angle of sideslip, rad
Δt_{f}	=	Projectile total flight time, s
$\Delta t_{\mathrm{un}}, \tilde{\Delta} t_{\mathrm{un}}, \hat{\Delta} t_{\mathrm{un}}^*$	=	Instability time period, approximated instability time periods, s
ρ	=	Air density, kg/m^3
ϕ, θ, ψ	=	Roll, pitch, yaw Euler angles, rad
$\boldsymbol{\omega}^{\mathrm{be}}$	=	Projectile body frame angular velocity vector wrt to earth frame
$\boldsymbol{\Omega}^{\mathrm{be}}$	=	Projectile body frame angular velocity tensor wrt to earth frame

I. Introduction

The field of guided artillery projectiles has attracted increased interest over the last few years due mostly to increased requirements concerning delivery accuracy in order to decrease dispersion and thus collateral damage as well as round expenditure. Open-loop unguided projectile launch is becoming progressively obsolete since the practice of pre-calculating the projectile impact point using only data tables and wind measurements is not always accurate due to uncertain launch and weather conditions. In addition, other uncertainties stemming from weapon misalignments, mishandlements and rough treatment from military personnel during battle may aggravate this situation.

A potential and promising solution to this problem is the use of closed-loop feedback guidance and control schemes in order to attenuate the effects of this uncertainty, thus optimizing overall weapon performance. These control schemes may use various types of aerodynamic control surfaces such as speed and drag brakes, deflection canards, or even jet thrusters to correct a projectile's trajectory. As far as control algorithms are concerned, various feasibility studies have been conducted.[3,9,10] In addition a number of robust-optimal control[13,15,21] and predictive control[2,22] schemes have been proposed over the years. There remains however much to be done in this field; especially when comparing to the vast existing bibliography for missile and aircraft control, with methods spanning LTI control, advanced LPV, adaptive and even pure nonlinear control (see for example Refs. 1, 23 and references therein).

For the purpose of regulating a projectile trajectory through the synthesis of appropriate control laws, the availability of both a sufficiently accurate but simple enough linear model of the system is of crucial importance. These linear models may be obtained either by locally linearizing the nonlinear dynamics about a single operating point (thus resulting in a LTI system) or about a flight envelope containing a theoretically infinite number of operating points (thus resulting in a LPV model). In the existing spinning projectile literature, this distinction is not always visible and may sometimes give models of limited validity. In addition, trimming values for the states are commonly obtained by performing ad-hoc assumptions, such as constant roll rates and longitudinal velocities throughout the projectile trajectory, or even by neglecting lateral velocities and rates or considering constant aerodynamic coefficients. Even though there exists considerable work on the topic,[4,11,17,18] this paper introduces a more accurate method of obtaining a LTV model of a spinning projectile using the body-rolling frame.

This method is based on the classic trajectory/solution-based linearization theory, where a generic nonlinear dynamical system is approximated along a tube about a given reference state trajectory solution $\mathcal{T}_{\mathrm{r}}$.[7,19] This trajectory, being the result of an initial launch state conditions set, constitutes in fact the actual trim condition, since it satisfies the nonlinear system dynamics for a given time period. The nonlinear dynamics are then linearized along this trajectory using a complete analytic Jacobian linearization with respect to the state vector, resulting thus in a LTV system. The terms considered are the ones with a significant contribution to each partial derivative element. The contribution is assessed using numerical linearization routines which provide a LTI model of the nonlinear dynamics at a large number of pre-defined time instants during the projectile flight time. It follows that an accurate LTV model may be thus obtained by considering time instants sufficiently close to one another.

In this work the body-rolling frame is used since it is more physically intuitive as it follows the spinning projectile's rolling motion. Its drawback, however, is that it provides heavily oscillating state variables which can lead to large simulation times. It is obvious that this approach may be also applied to the more standard non-rolling body frame. In addition, it may easily take into account any control surfaces or actuators subsequently incorporated into the open-loop model.

The LTV model obtained through linearization may then be used in order to assess the projectile stability properties, which are often complicated or not sufficiently accurate when classic aeroballistic stability theory is preferred. The stability analysis for a generic nonlinear system is no easy problem; however it may be sometimes feasible to perform such an analysis using linear models of this system at distinct time instances. Calculating the eigenvalues of the resulting models yields in general sufficient knowledge concerning the instability phases of the LTV, and thus of the initial nonlinear model. In this work, a thorough treatment of the problem is performed and some simple conditions approximating the stable phase of the projectile flight are obtained.

In the present paper, Section II presents a full nonlinear mathematical model for the translation and rotation dynamics subsystem of an unguided spin-stabilized projectile in the body-rolling frame; illustrative simulation results concerning its 3D trajectory are also provided. Section III reviews the trajectory-based linearization framework of a generic nonlinear dynamical system and then presents its application on the projectile dynamics subsystem resulting thus in a LTV state space model. The internal structure of this model is analyzed in Section IV and the results are regrouped in appropriate state space matrices. Finally, in Section V are discussed some stability properties of the aforementioned state space model; this discussion involves a complement of frozen-time eigenvalue analysis, numerical computations and a comparison to classic aeroballistic stability analysis.

II. Projectile Modeling

In this section we present the equations of motion that model the projectile's atmospheric trajectory according to a set of initial launch conditions. The translation dynamics give the projectile linear velocity as a result of the externally applied forces, whereas the attitude dynamics give its angular velocity as a function of the corresponding moments. In this work, a tensor formulation[25] of the Newton-Euler equations is used since it is valid in any coordinate system and thus allows a rigorous treatment.

A. Translation Dynamics

Assuming a short flight time, the earth may be considered to be an inertial-reference frame, and Newton's second law gives the time-derivative of the projectile body's linear velocity vector $\mathbf{v}_{\mathrm{b}}^{\mathrm{e}}$ with respect to the earth-inertial frame as a function of the externally applied force vector $\mathbf{F}$, angular velocity tensor of the body frame with respect to the inertial frame $\mathbf{\Omega}^{\mathrm{be}}$ and vehicle mass m, with the symbol $\mathscr{D}^{\mathrm{b}}$ denoting time derivation with respect to the body frame:

$$\mathscr{D}^{\mathrm{b}}\mathbf{v}_{\mathrm{b}}^{\mathrm{e}} = -\mathbf{\Omega}^{\mathrm{be}}\mathbf{v}_{\mathrm{b}}^{\mathrm{e}} + \frac{1}{m}\mathbf{F}. \tag{1}$$

The body frame is chosen since the externally applied forces are a function of the incidence angles which are calculated from the velocity vector as perceived from the vehicle as a reference frame. Equation (1) should also be expressed in a preferable coordinate system since actual variable values are needed for simulation. The coordinate system used the body-rolling noted $[\cdot]^{\mathrm{b}}$ and Equation (1) thus becomes:

$$\left[\frac{\mathrm{d}\mathbf{v}_{\mathrm{b}}^{\mathrm{e}}}{\mathrm{d}t}\right]^{\mathrm{b}} = -\left[\mathbf{\Omega}^{\mathrm{be}}\right]^{\mathrm{b}}\left[\mathbf{v}_{\mathrm{b}}^{\mathrm{e}}\right]^{\mathrm{b}} + \frac{1}{m}\left[\mathbf{F}\right]^{\mathrm{b}}. \tag{2}$$

Equation (2) is in tensor form, hence for example $\left[\mathbf{v}_{\mathrm{b}}^{\mathrm{e}}\right]^{\mathrm{b}}$ denotes the projectile linear velocity vector $[u \quad v \quad w]^{\top}$. The coordinate systems listed in Table (1) are the earth-inertial, velocity and body ones. In order to model the forces and moments applied to the projectile, we use the unitary vectors $[\mathbf{v}_1]^{\mathrm{b}}, [\mathbf{b}_1]^{\mathrm{b}}, [\mathbf{e}_3]^{\mathrm{b}}$; however $[\mathbf{v}_1]^{\mathrm{b}}, [\mathbf{e}_3]^{\mathrm{b}}$ need to be computed in the velocity and inertial coordinate systems respectively, and thus two transformation matrices $[\mathbf{T}]^{\mathrm{bv}}, [\mathbf{T}]^{\mathrm{be}}$ are needed since:

$$[\mathbf{v}_1]^{\mathrm{b}} \triangleq [\mathbf{T}]^{\mathrm{bv}}[\mathbf{v}_1]^{\mathrm{v}}, \tag{3}$$

$$[\mathbf{e}_3]^{\mathrm{b}} \triangleq [\mathbf{T}]^{\mathrm{be}}[\mathbf{e}_3]^{\mathrm{e}}, \tag{4}$$

and:

$$[\mathbf{b}_1]^{\mathrm{b}} \triangleq \begin{bmatrix}1\\0\\0\end{bmatrix}^{\mathrm{b}}, \; [\mathbf{v}_1]^{\mathrm{v}} \triangleq \begin{bmatrix}1\\0\\0\end{bmatrix}^{\mathrm{v}}, \; [\mathbf{e}_3]^{\mathrm{e}} \triangleq \begin{bmatrix}0\\0\\1\end{bmatrix}^{\mathrm{e}}. \tag{5}$$

The transformation from the body to the velocity coordinate system is done by rotating first by $-\alpha$ about the $\mathbf{b}_2$ axis and then by β thus resulting to $[\mathbf{T}]^{\mathrm{vb}}$; the transformation matrix $[\mathbf{T}]^{\mathrm{bv}}$ is simply calculated by transposing $[\mathbf{T}]^{\mathrm{vb}}$. The transformation from the earth-inertial to the body frame is done by rotating successively by the Euler angles ψ, θ, ϕ, thus leading to $[\mathbf{T}]^{\mathrm{be}}$. After performing all the necessary calculations we obtain the following rotation matrices:[25]

$$[\mathbf{T}]^{\mathrm{bv}} = \begin{bmatrix} c_\alpha c_\beta & -c_\alpha s_\beta & -s_\alpha \\ s_\beta & c_\beta & 0 \\ s_\alpha c_\beta & -s_\alpha s_\beta & c_\alpha \end{bmatrix}, \tag{6}$$

$$[\mathbf{T}]^{\mathrm{be}} = \begin{bmatrix} c_\theta c_\psi & c_\theta s_\psi & -s_\theta \\ s_\phi s_\theta c_\psi - c_\phi s_\psi & s_\phi s_\theta s_\psi + c_\phi c_\psi & s_\phi c_\theta \\ c_\phi s_\theta c_\psi + s_\phi s_\psi & c_\phi s_\theta s_\psi - s_\phi c_\psi & c_\phi c_\theta \end{bmatrix}. \tag{7}$$

The AoA α is defined as the angle between the projection of the velocity vector onto the $\mathbf{b}_1 - \mathbf{b}_3$ plane and the $\mathbf{b}_1$ base vector, with the aforementioned projection defining the AoS angle β. In addition, the angle between the base vectors $\mathbf{v}_1$ and $\mathbf{b}_1$ defines the total aeroballistic incidence angle α_{t}:

$$\alpha_{\mathrm{t}} \triangleq \arcsin\sqrt{1 - \frac{1}{\sec^2\alpha + \tan^2\beta}}. \tag{8}$$

Finally, the projectile airspeed is calculated as:

$$V = \sqrt{u^2 + v^2 + w^2}. \tag{9}$$

Table 1. Preferred coordinate systems

Coordinate system	Base vectors	Explanation
Earth-inertial	$\mathbf{e}_1$	northwards
	$\mathbf{e}_2$	eastwards
	$\mathbf{e}_3$	towards gravity
Velocity	$\mathbf{v}_1$	on the velocity vector
	$\mathbf{v}_2$	normal to $\mathbf{v}_1$, non-rotating
	$\mathbf{v}_3$	right-hand rule
Body	$\mathbf{b}_1$	on the projectile axis
	$\mathbf{b}_2$	normal to $\mathbf{b}_1$, rotating
	$\mathbf{b}_3$	right-hand rule

1. *Drag Force*

The drag force $\mathbf{F}_\mathrm{D}$ applied to the center of pressure $\mathrm{CP_f}$ is created due to the projectile airspeed V and is modeled using the corresponding aerodynamic coefficient $C_\mathrm{D}(\alpha_\mathrm{t}, M)$ which increases with the projectile's aeroballistic AoA α_t. This force is written in the body coordinate system as:

$$\begin{aligned}\left[\mathbf{F}_\mathrm{D}\right]^\mathrm{b} &= -\overline{q}SC_\mathrm{D}(\alpha_\mathrm{t}, M)\,[\mathbf{v}_1]^\mathrm{b} = -\overline{q}SC_\mathrm{D}(\alpha_\mathrm{t}, M)\,[\mathbf{T}]^\mathrm{bv}[\mathbf{v}_1]^\mathrm{v} \\ &= -\overline{q}SC_\mathrm{D}(\alpha_\mathrm{t}, M)\begin{bmatrix} c_\alpha c_\beta \\ s_\beta \\ s_\alpha c_\beta \end{bmatrix}^\mathrm{b},\end{aligned} \tag{10}$$

where $\overline{q} = \frac{1}{2}\,\rho V^2$ denotes the dynamic pressure defined using the altitude-dependent air density ρ.

2. *Lift Force*

The lift force $\mathbf{F}_\mathrm{L}$ applied also to $\mathrm{CP_f}$ is perpendicular to the trajectory and tends to pull the projectile towards the direction in which its nose is pointed.[18] The corresponding lift aerodynamic coefficient $C_{\mathrm{L}\alpha}(\alpha_\mathrm{t}, M)$ increases with the projectile's airspeed. This force is written in the body coordinate system as:

$$\begin{aligned}\left[\mathbf{F}_\mathrm{L}\right]^\mathrm{b} &= \overline{q}SC_{\mathrm{L}\alpha}(\alpha_\mathrm{t}, M)\,[\mathbf{v}_1]^\mathrm{b} \times \left([\mathbf{b}_1]^\mathrm{b} \times [\mathbf{v}_1]^\mathrm{b}\right) \\ &= \overline{q}SC_{\mathrm{L}\alpha}(\alpha_\mathrm{t}, M)\begin{bmatrix} s_\beta^2 + s_\alpha^2 c_\beta^2 \\ -c_\alpha s_\beta c_\beta \\ -s_\alpha c_\alpha c_\beta^2 \end{bmatrix}^\mathrm{b}.\end{aligned} \tag{11}$$

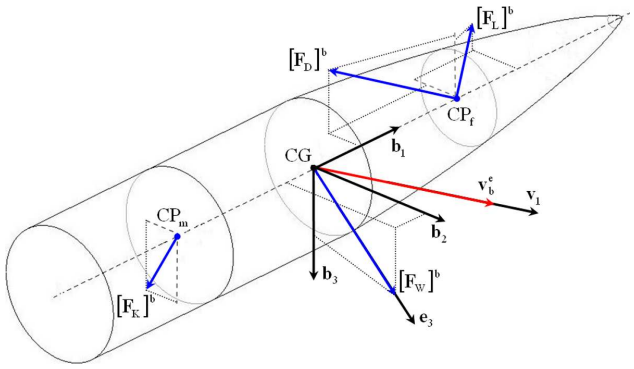

Figure 1. Forces acting on the projectile.

3. Magnus Force

The Magnus force $\mathbf{F}_{\mathrm{K}}$ is due to the large projectile rotational velocity leading to uneven opposite side pressure distributions. It is applied to the Magnus center of pressure $\mathrm{CP_m}$, with the corresponding Magnus force coefficient $C_{yp\alpha}(M)$ being generally difficult to precisely quantify. The Magnus force is proportional to the roll (or spinning) velocity p which constitutes the first component of the projectile angular velocity with respect to the inertial frame expressed in body coordinates $[\boldsymbol{\omega}_{\mathrm{b}}^{\mathrm{e}}]^{\mathrm{b}}$. The Magnus force is written as:

$$\begin{aligned}\left[\mathbf{F}_{\mathrm{K}}\right]^{\mathrm{b}} &= \overline{q}S\left(\frac{d}{V}\right)C_{yp\alpha}(M)p\,[\mathbf{b}_1]^{\mathrm{b}} \times [\mathbf{v}_1]^{\mathrm{b}} \\ &= \overline{q}S\left(\frac{d}{V}\right)C_{yp\alpha}(M)p\begin{bmatrix}0\\ -s_\alpha c_\beta\\ s_\beta\end{bmatrix}^{\mathrm{b}}.\end{aligned} \tag{12}$$

4. Gravity Force

The gravity force $\mathbf{F}_{\mathrm{W}}$ is applied to the center of gravity CG and is simply written in the body coordinate system as:

$$\begin{aligned}\left[\mathbf{F}_{\mathrm{W}}\right]^{\mathrm{b}} &= mg\,[\mathbf{e}_3]^{\mathrm{b}} = mg\,[\mathbf{T}]^{\mathrm{be}}[\mathbf{e}_3]^{\mathrm{e}} \\ &= mg\begin{bmatrix}-s_\theta\\ s_\phi c_\theta\\ c_\phi c_\theta\end{bmatrix}^{\mathrm{b}}.\end{aligned} \tag{13}$$

B. Rotation Dynamics

Concerning the rotation dynamics, Euler's law states that the time rate of change of angular momentum is equal to the externally applied moments. Stating the law with respect to the body frame, we have the following relationship:

$$\mathscr{D}^{\mathrm{b}}\boldsymbol{\omega}^{\mathrm{be}} = -\left(\mathbf{I}_{\mathrm{b}}^{\mathrm{b}}\right)^{-1}\boldsymbol{\Omega}^{\mathrm{be}}\mathbf{I}_{\mathrm{b}}^{\mathrm{b}}\boldsymbol{\omega}^{\mathrm{be}} + \left(\mathbf{I}_{\mathrm{b}}^{\mathrm{b}}\right)^{-1}\mathbf{M}_{\mathrm{b}}. \tag{14}$$

where $\boldsymbol{\omega}^{\mathrm{be}}$ is the body frame angular velocity vector with respect to the inertial frame, $\mathbf{M}_{\mathrm{b}}$ denotes the external moment vector and $\mathbf{I}_{\mathrm{b}}^{\mathrm{b}}$ is the projectile MOI tensor, both referred to CG. Similarly to the translation dynamics, we choose the body coordinate system and thus the simulation equations become:

$$\left[\frac{\mathrm{d}\boldsymbol{\omega}^{\mathrm{be}}}{\mathrm{d}t}\right]^{\mathrm{b}} = -\left(\left[\mathbf{I}_{\mathrm{b}}^{\mathrm{b}}\right]^{\mathrm{b}}\right)^{-1}\left[\boldsymbol{\Omega}^{\mathrm{be}}\right]^{\mathrm{b}}\left[\mathbf{I}_{\mathrm{b}}^{\mathrm{b}}\right]^{\mathrm{b}}\left[\boldsymbol{\omega}^{\mathrm{be}}\right]^{\mathrm{b}} + \left(\left[\mathbf{I}_{\mathrm{b}}^{\mathrm{b}}\right]^{\mathrm{b}}\right)^{-1}\left[\mathbf{M}_{\mathrm{b}}\right]^{\mathrm{b}}. \tag{15}$$

1. Pitch-Yaw Moment

The pitch-yaw moment $\mathbf{M}_{\mathrm{PY}}$ is created by the combination of the lift and drag forces applied to the center of pressure $\mathrm{CP_f}$, and is modeled using the corresponding aerodynamic function $C_{\mathrm{m}\alpha}(\alpha_{\mathrm{t}}, M)$. Since the projectile has no lifting surfaces $C_{\mathrm{m}\alpha}(\alpha_{\mathrm{t}}, M) > 0$. This moment is written:

$$\begin{aligned}\left[\mathbf{M}_{\mathrm{PY}}\right]^{\mathrm{b}} &= \overline{q}SdC_{\mathrm{m}\alpha}(\alpha_{\mathrm{t}}, M)\,[\mathbf{v}_1]^{\mathrm{b}} \times [\mathbf{b}_1]^{\mathrm{b}} \\ &= \overline{q}SdC_{\mathrm{m}\alpha}(\alpha_{\mathrm{t}}, M)\begin{bmatrix}0\\ s_\alpha c_\beta\\ -s_\beta\end{bmatrix}^{\mathrm{b}}.\end{aligned} \tag{16}$$

2. Magnus Moment

The Magnus moment $\mathbf{M}_{\mathrm{M}}$ is the resultant of the Magnus force applied at the Magnus center of pressure $\mathrm{CP_m}$. This moment is also dependent on the roll velocity p, and is modeled using an aerodynamic function $C_{\mathrm{n}p\alpha}(M)$ whose sign may change with the airspeed:

$$\begin{aligned}\left[\mathbf{M}_{\mathrm{K}}\right]^{\mathrm{b}} &= \overline{q}Sd\left(\frac{d}{V}\right)C_{\mathrm{n}p\alpha}(M)p\,[\mathbf{b}_1]^{\mathrm{b}} \times \left([\mathbf{b}_1]^{\mathrm{b}} \times [\mathbf{v}_1]^{\mathrm{b}}\right) \\ &= \overline{q}Sd\left(\frac{d}{V}\right)C_{\mathrm{n}p\alpha}(M)p\begin{bmatrix}0\\ -s_\beta\\ -s_\alpha c_\beta\end{bmatrix}^{\mathrm{b}}.\end{aligned} \tag{17}$$

3. *Damping Roll & Pitch-Yaw Moments*

The damping roll moment $\mathbf{M}_{\mathrm{Rd}}$ is proportional to the spinning velocity p, tending to reduce it along the trajectory. The corresponding aerodynamic coefficient $C_{\mathrm{l}p}(M)$ is always negative and thus this moment is written:

$$\begin{aligned}\left[\mathbf{M}_{\mathrm{Rd}}\right]^{\mathrm{b}} &= \overline{q}Sd\left(\frac{d}{V}\right)C_{\mathrm{l}p}(M)p\,\left[\mathbf{b}_1\right]^{\mathrm{b}} \\ &= \overline{q}Sd\left(\frac{d}{V}\right)C_{\mathrm{l}p}(M)p\begin{bmatrix}1\\0\\0\end{bmatrix}^{\mathrm{b}}.\end{aligned} \tag{18}$$

The damping pitch-yaw moment $\mathbf{M}_{\mathrm{PYd}}$ depends on the pitch-yaw axes rotational velocities q and r with the corresponding aerodynamic coefficient $C_{\mathrm{m}q}(M)$ being also negative. This moment is written:

$$\begin{aligned}\left[\mathbf{M}_{\mathrm{PYd}}\right]^{\mathrm{b}} &= \overline{q}Sd\left(\frac{d}{V}\right)C_{\mathrm{m}q}(M)\,\left[\mathbf{b}_1\right]^{\mathrm{b}}\times\left(\left[\boldsymbol{\omega}^{\mathrm{be}}\right]^{\mathrm{b}}\times\left[\mathbf{b}_1\right]^{\mathrm{b}}\right) \\ &= \overline{q}Sd\left(\frac{d}{V}\right)C_{\mathrm{m}q}(M)\begin{bmatrix}0\\q\\r\end{bmatrix}^{\mathrm{b}}.\end{aligned} \tag{19}$$

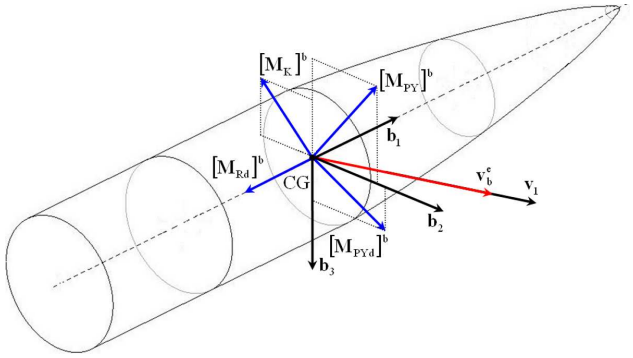

Figure 2. Moments acting on the projectile.

C. Nonlinear Equations of Motion and Simulations

Supposing that during the projectile trajectory $\alpha,\beta \lesssim 15^{\circ}$, then $s_\alpha \simeq \alpha, c_\alpha \simeq 1, s_\beta \simeq \beta, c_\beta \simeq 1$. The modeling presented so far is valid for perfectly symmetric projectiles; however this is not the case in reality so we prefer to use missile-type aerodynamic function notation and set $C_{\mathrm{D}} \equiv C_{\mathrm{A}}, -C_{\mathrm{L}\alpha} - C_{\mathrm{D}} \equiv C_{\mathrm{Y}\beta} = C_{\mathrm{N}\alpha}, C_{\mathrm{m}q} \equiv C_{\mathrm{n}r}, -C_{\mathrm{m}\alpha} \equiv C_{\mathrm{n}\beta}$. The constants $I_{\mathrm{x}}, I_{\mathrm{t}}$ are the projectile MOI tensor diagonal components, S denotes the projectile reference surface and d its caliber. The projectile's forces and moments equations are given by:

$$\dot{u} = rv - qw - gs_\theta - \frac{1}{m}\overline{q}SC_{\mathrm{A}}(\alpha_{\mathrm{t}}, M), \tag{20}$$

$$\dot{v} = pw - ru + gs_\phi c_\theta + \frac{1}{m}\overline{q}S\left[C_{\mathrm{Y}\beta}(\alpha_{\mathrm{t}}, M)\beta - \left(\frac{d}{V}\right)C_{\mathrm{yp}\alpha}(M)p\alpha\right], \tag{21}$$

$$\dot{w} = qu - pv + gc_\phi c_\theta + \frac{1}{m}\overline{q}S\left[C_{\mathrm{N}\alpha}(\alpha_{\mathrm{t}}, M)\alpha + \left(\frac{d}{V}\right)C_{\mathrm{yp}\alpha}(M)p\beta\right], \tag{22}$$

$$\dot{p} = \frac{1}{I_{\mathrm{x}}}\overline{q}Sd\left(\frac{d}{V}\right)C_{\mathrm{l}p}(M)p, \tag{23}$$

$$\dot{q} = \frac{I_{\mathrm{t}} - I_{\mathrm{x}}}{I_{\mathrm{t}}}rp + \frac{1}{I_{\mathrm{t}}}\overline{q}Sd\left[C_{\mathrm{m}\alpha}(\alpha_{\mathrm{t}}, M)\alpha + \left(\frac{d}{V}\right)C_{\mathrm{m}q}(M)q - \left(\frac{d}{V}\right)C_{\mathrm{np}\alpha}(M)p\beta\right], \tag{24}$$

$$\dot{r} = \frac{I_{\mathrm{x}} - I_{\mathrm{t}}}{I_{\mathrm{t}}}qp + \frac{1}{I_{\mathrm{t}}}\overline{q}Sd\left[C_{\mathrm{n}\beta}(\alpha_{\mathrm{t}}, M)\beta + \left(\frac{d}{V}\right)C_{\mathrm{n}r}(M)r - \left(\frac{d}{V}\right)C_{\mathrm{np}\alpha}(M)p\alpha\right]. \tag{25}$$

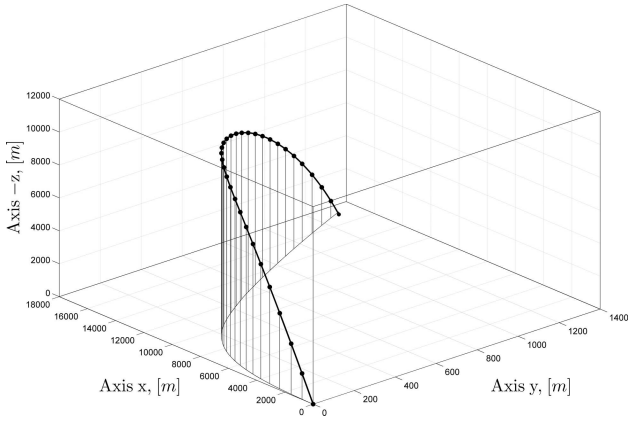

Figure 3. Projectile trajectory $[x_{\mathrm{e}}, y_{\mathrm{e}}, z_{\mathrm{e}}](t)$**.**

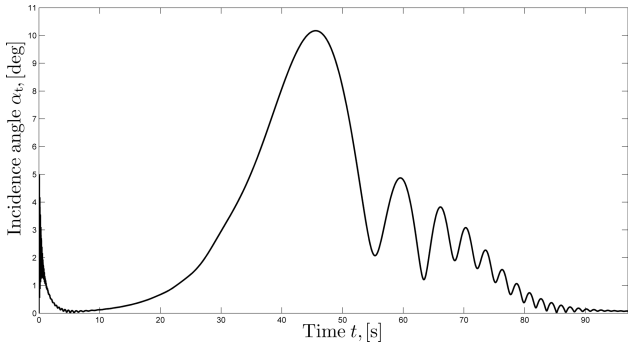

Figure 4. Aeroballistic incidence angle $\alpha_{\mathrm{t}}(t)$**.**

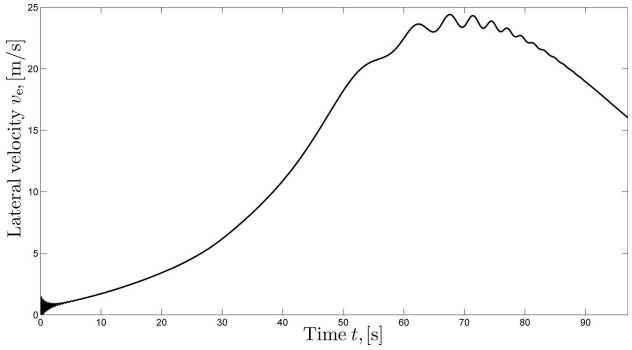

Figure 5. Lateral velocity $v_{\mathrm{e}}(t)$**.**

The forces and moments equations need to be complemented by the following set of six kinematics equations, describing the Euler angles $[\mathbf{e}^{\mathrm{be}}]^{\mathrm{e}} = [\phi \quad \theta \quad \psi]^{\top}$ and the projectile's displacement $[\mathbf{s}_{\mathrm{be}}]^{\mathrm{e}} = [x_{\mathrm{e}} \quad y_{\mathrm{e}} \quad z_{\mathrm{e}}]^{\top}$ vectors rate of change expressed in the inertial frame:

$$\dot{\phi} = p + s_{\phi} t_{\theta} q + c_{\phi} t_{\theta} r, \tag{26}$$

$$\dot{\theta} = c_{\phi} q - s_{\phi} r, \tag{27}$$

$$\dot{\psi} = s_{\phi}/c_{\theta} q + c_{\phi}/c_{\theta} r, \tag{28}$$

$$\dot{x}_{\mathrm{e}} = c_{\theta} c_{\psi} u + (s_{\phi} s_{\theta} c_{\psi} - c_{\phi} s_{\psi}) v + (c_{\phi} s_{\theta} c_{\psi} + s_{\phi} s_{\psi}) w, \tag{29}$$

$$\dot{y}_{\mathrm{e}} = c_{\theta} s_{\psi} u + (s_{\phi} s_{\theta} s_{\psi} + c_{\phi} c_{\psi}) v + (c_{\phi} s_{\theta} s_{\psi} - s_{\phi} c_{\psi}) w, \tag{30}$$

$$\dot{z}_{\mathrm{e}} = -s_{\theta} u + s_{\phi} c_{\theta} v + c_{\phi} c_{\theta} w. \tag{31}$$

Simulating the dynamics and kinematics equations with the initial launch state condition $p_0 \approx 1600\frac{\text{rad}}{\text{s}}, r_0 \approx -3\frac{\text{rad}}{\text{s}}, \theta_0 \approx 60^\circ, u_0 \approx 800\frac{\text{m}}{\text{s}}$, we obtain Figures (3)-(5) showing the projectile trajectory, aeroballistic incidence angle and lateral velocity. Figure (3) shows that the projectile has the tendency to deviate to the right due to the rapid rolling motion; this observation is also confirmed by Figure (5), which demonstrates a positive lateral velocity v_e. Finally, Figure (4) shows that, during an important time window, the aeroballistic incidence angle reaches a rather significant amplitude; this fact being an indicator of instability as will be discussed in Section V.

III. Trajectory-based Linearization

In this section we present the main results of the paper which include a more accurate method of derivation of the projectile's linearized dynamics about a trajectory and a comprehensive but simple stability study using frozen-time eigenvalue analysis.

A. Linearization Framework

Consider the following forced autonomous nonlinear system $\mathscr{S}$:

$$\mathscr{S}: \quad \dot{\mathbf{x}}(t) = \mathbf{f}\big[\mathbf{x}(t), \mathbf{u}(t)\big] \tag{32}$$

where $\mathbf{x}(t) = \mathbf{x}(t; \mathbf{x}_0, t_0) \in \mathscr{R}^n, t_0 \geq 0$ is the system's state vector, $\mathbf{x}_0 = \mathbb{O}_n$ denotes the initial state conditions (this analysis is also valid for non-zero initial state conditions through a change of coordinates), $\mathbf{u}(t) \in \mathscr{R}^m$ the control input, and $\mathbf{f} : \mathscr{R}^n \times \mathscr{R}^m \mapsto \mathscr{R}^n$ a continuous vector-valued nonlinear function satisfying appropriate conditions such that a solution to Equation (32) exists and is unique.[14,24] The general goal when linearizing the system $\mathscr{S}$ is to obtain another, essentially linear system $\hat{\mathscr{S}}$, whose solution will be comparatively easier to calculate, and will approximate $\mathbf{x}(t)$ with the necessary accuracy under certain assumptions.

Suppose that under a generally time-varying reference (or bias) input $\mathbf{u}_\text{r}(t)$, the system $\mathscr{S}$ admits a solution (or reference trajectory) $\mathbf{x}_\text{r}(t)$ satisfying Equation (32). Suppose also (e.g. for the sake of controlling the plant $\mathscr{S}$) that the total system input is the sum of the bias input and of a control input $\mathbf{u}_\delta(t)$ such that:

$$\mathbf{u}(t) = \mathbf{u}_\text{r}(t) + \mathbf{u}_\delta(t). \tag{33}$$

Similar to the control input, the state trajectory can be also written as the sum of the reference one $\mathbf{x}_\text{r}(t)$ plus a 'perturbed' one $\mathbf{x}_\delta(t)$:

$$\mathbf{x}(t) = \mathbf{x}_\text{r}(t) + \mathbf{x}_\delta(t). \tag{34}$$

If now $\mathbf{x}_\text{r}(t)$ is known and $\mathbf{x}_\delta(t)$ could be easily calculated or approximated, then the actual state trajectory $\mathbf{x}(t)$ may be computed (or approximated) without having to solve the initial nonlinear dynamics of Equation (32). Furthermore, under some conditions,[7,8,16] the perturbed state component $\mathbf{x}_\delta(t)$ may be approximated by the state solution $\hat{\mathbf{x}}_\delta(t)$ of the non-autonomous LTV forced system $\hat{\mathscr{S}}$:

$$\hat{\mathscr{S}}: \quad \dot{\hat{\mathbf{x}}}_\delta(t) = \mathbf{A}(t)\hat{\mathbf{x}}_\delta(t) + \mathbf{B}(t)\mathbf{u}_\delta(t), \tag{35}$$

where the time-varying system matrices $\mathbf{A}(t) \in \mathscr{R}^{n\times n}$ and $\mathbf{B}(t) \in \mathscr{R}^{n\times m}$ are defined as the first order partial derivatives of $\mathbf{f} := [f_1, f_2, \ldots, f_n]^\top$ with respect to the state and the input respectively, and are evaluated *along the reference system trajectory* $\mathcal{T}_\text{r} : \{\mathbf{x}_\text{r}(t), \mathbf{u}_\text{r}(t)\}$. Thus:

$$\mathbf{A}(t) \triangleq \nabla_\mathbf{x}\mathbf{f}\big|_{\mathcal{T}_\text{r}}, \tag{36}$$

$$\mathbf{B}(t) \triangleq \nabla_\mathbf{u}\mathbf{f}\big|_{\mathcal{T}_\text{r}}, \tag{37}$$

with:

$$\nabla_\mathbf{x}\mathbf{f} = \begin{bmatrix} \nabla_{x_1} f_1 & \ldots & \nabla_{x_n} f_1 \\ \ldots & \ddots & \ldots \\ \nabla_{x_1} f_n & \ldots & \nabla_{x_n} f_n \end{bmatrix}, \quad \nabla_\mathbf{u}\mathbf{f} = \begin{bmatrix} \nabla_{u_1} f_1 & \ldots & \nabla_{u_m} f_1 \\ \ldots & \ddots & \ldots \\ \nabla_{u_1} f_n & \ldots & \nabla_{u_m} f_n \end{bmatrix}. \tag{38}$$

In the context of this work, and supposing that a projectile remains within a neighborhood of a pre-described open-loop state trajectory $\mathbf{x}_\text{r}(t)$ as a result of given non-zero initial launch conditions, then its 'small signal' behavior within a tube enveloping $\mathcal{T}_\text{r}$ may be approximated by the LTV system $\hat{\mathscr{S}}$. Note that $\mathbf{u}_\text{r}(t)$ denotes the bias control input which would maintain the state on the reference state trajectory $\mathbf{x}_\text{r}(t)$ (commonly called trim control). In our case however, there are no control surfaces since the projectile is studied in open-loop and hence $\mathbf{u}(t) = \mathbf{u}_\text{r}(t) \equiv 0, \forall t \geq t_0$. Using this linearization, a stability analysis of the resulting projectile reference state trajectory may be conducted using the linear model $\hat{\mathscr{S}}$ as it will be discussed in Section V.

B. Projectile Dynamics Linearization

In the following, the projectile model state vector $\mathbf{x}$ is decomposed in the dynamics and kinematics state vectors:

$$\mathbf{x} \triangleq \begin{bmatrix} \mathbf{x}_{\mathrm{d}} \\ \mathbf{x}_{\mathrm{k}} \end{bmatrix} \tag{39}$$

where $\mathbf{x}_{\mathrm{d}} = \begin{bmatrix} p & q & r & u & v & w \end{bmatrix}^{\top}$ and $\mathbf{x}_{\mathrm{k}} = \begin{bmatrix} \phi & \theta & \psi & x_{\mathrm{e}} & y_{\mathrm{e}} & z_{\mathrm{e}} \end{bmatrix}^{\top}$. Since the projectile dynamics are studied in open-loop $\mathbf{u} = 0$, and thus linearization around the state trajectory solution $\mathbf{x}_{\mathrm{r}}$ will yield the following unforced nonautonomous LTV system (the hat notation is removed under the assumption that $\hat{\mathbf{x}}_{\delta} \rightarrow \mathbf{x}_{\delta}$):

$$\mathscr{S}_{\mathbf{x}} : \quad \dot{\mathbf{x}}_{\delta} = \mathbf{A}(t)\mathbf{x}_{\delta} \tag{40}$$

where $\mathbf{A}(t) \triangleq \nabla_{\mathbf{x}}\mathbf{f}\big|_{\mathbf{x}_{\mathrm{r}}}$. The vector-valued nonlinear function $\mathbf{f} := \mathbf{f}[\mathbf{x}(t)] = [f_p, f_q, \ldots, f_{z_{\mathrm{e}}}]^{\top}$ contains the right-hand sides of Equations (20)-(31), ordered in accordance to the state vector $\mathbf{x}$ of Equation (39). Each of the following paragraphs focuses only on the linearization of the dynamics subsystem since linearization of the kinematics equations is standard. Equation (40) may be decomposed as:

$$\begin{bmatrix} \dot{\mathbf{x}}_{\mathrm{d}\delta} \\ \dot{\mathbf{x}}_{\mathrm{k}\delta} \end{bmatrix} = \left[\begin{array}{c|c} \mathbf{A}_{\mathrm{dd}}(t) & \mathbf{A}_{\mathrm{dk}}(t) \\ \hline \mathbf{A}_{\mathrm{kd}}(t) & \mathbf{A}_{\mathrm{kk}}(t) \end{array}\right] \begin{bmatrix} \mathbf{x}_{\mathrm{d}\delta} \\ \mathbf{x}_{\mathrm{k}\delta} \end{bmatrix} \tag{41}$$

where we are mainly interested in the matrices $\mathbf{A}_{\mathrm{dd}}(t), \mathbf{A}_{\mathrm{dk}}(t) \in \mathscr{R}^{6\times 6}$, since they prove sufficient in order to characterize system stability. The linear state dynamics for $\mathbf{x}_{\mathrm{d}\delta}$ are:

$$\mathscr{S}_{\mathbf{x}_{\mathrm{d}}} : \quad \dot{\mathbf{x}}_{\mathrm{d}\delta} = \mathbf{A}_{\mathrm{dd}}(t)\mathbf{x}_{\mathrm{d}\delta} + \mathbf{A}_{\mathrm{dk}}(t)\mathbf{x}_{\mathrm{k}\delta}. \tag{42}$$

A partial stability analysis of the projectile dynamics may be performed by studying the properties of the LTV system $\mathscr{S}_{x_{\mathrm{d}}}$ by computing the eigenvalues of the stability matrix $\mathbf{A}_{\mathrm{dd}}(t)$ and considering the second part of Equation (42) as an external perturbation $\mathbf{w}(t)$ as illustrated in Figure (6).

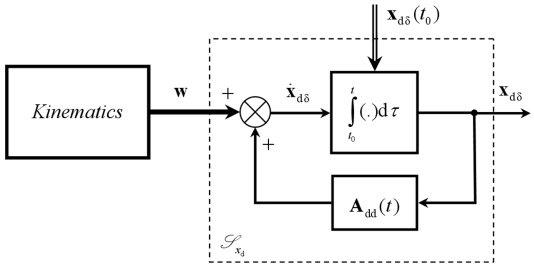

Figure 6. Dynamics subsystem.

1. *Roll velocity linearization*

From Equation (23), it can be seen that f_p is a function of p, V and M; since $M = V/a$ where $a = a(z_{\mathrm{e}})$ is the altitude dependent speed of sound, $V = V(u, v, w)$ and $\overline{q} = \overline{q}(V, z_{\mathrm{e}}) = \frac{1}{2}\rho(z_{\mathrm{e}})V^2$, the Jacobian $\nabla_{\mathbf{x}} f_p$ needs only be computed for p, u, v, w and z_{e} since the other terms are zero. We begin with $\nabla_p f_p$:

$$\nabla_p f_p = \frac{1}{I_{\mathrm{x}}}\overline{q}Sd\left(\frac{d}{V}\right)C_{\mathrm{l}p}(M). \tag{43}$$

Derivation with respect to u, v and w is more difficult since $V = V(u, v, w)$. We first rewrite Equation (23) as $f_p = \frac{1}{2I_{\mathrm{x}}}\rho Sd^2 p V C_{\mathrm{l}p}(M)$, thus isolating the terms depending on V. The derivative $\nabla_u f_p$ is then of the form:

$$\nabla_u f_p = \frac{1}{2I_{\mathrm{x}}}\rho Sd^2 p\, \nabla_u\Big[VC_{\mathrm{l}p}(M)\Big]. \tag{44}$$

Since $\nabla_u V = \frac{u}{V}$ the derivative term of Equation (44) becomes:

$$\begin{aligned} \nabla_u\Big[VC_{\mathrm{l}p}(M)\Big] &= C_{\mathrm{l}p}(M)\nabla_u V + V\nabla_u C_{\mathrm{l}p}(M) \\ &= \frac{u}{V}\Big[C_{\mathrm{l}p}(M) + M\nabla_M C_{\mathrm{l}p}(M)\Big]. \end{aligned} \tag{45}$$

Substituting Equation (45) into Equation (44) and regrouping accordingly we obtain:

$$\nabla_u f_p = \frac{1}{I_x}\overline{q}Sd\left(\frac{d}{V}\right)\frac{u}{V^2}\Big[\, C_{lp}(M) + M\nabla_M C_{lp}(M)\Big]p. \tag{46}$$

For the v and w velocities, the analysis is similar and leads to:

$$\nabla_v f_p = \frac{1}{I_x}\overline{q}Sd\left(\frac{d}{V}\right)\frac{v}{V^2}\Big[\, C_{lp}(M) + M\nabla_M C_{lp}(M)\Big]p, \tag{47}$$

$$\nabla_w f_p = \frac{1}{I_x}\overline{q}Sd\left(\frac{d}{V}\right)\frac{w}{V^2}\Big[\, C_{lp}(M) + M\nabla_M C_{lp}(M)\Big]p. \tag{48}$$

The analysis performed in most works does not take into account the aerodynamic function derivative $\nabla_M C_{lp}(M)$ as presented in the above equations. Using MATLAB® and its numerical linearization tools, it can be shown that this is acceptable for $\nabla_v f_p, \nabla_w f_p$. However, in the case of $\nabla_u f_p$ there exists a significant difference as illustrated by Figure (7).

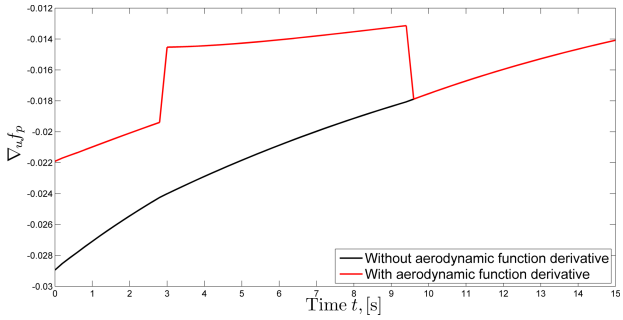

Figure 7. Comparison for $\nabla_u f_p$.

To compute $\nabla_{z_e} f_p$, even though this term is rather small, we need the partial derivatives of $\rho(z_e)$ and $C_{lp}(M)$ with respect to z_e. Again, numerical techniques highlight the fact that linearization with respect to the aerodynamic function could be neglected. Accordingly, the following expression is obtained:

$$\nabla_{z_e} f_p = \frac{1}{2I_x}SdV^2\left(\frac{d}{V}\right)C_{lp}(M)\nabla_{z_e}\rho\, p. \tag{49}$$

2. Pitch Velocity Linearization

Using Equation (24), the derivatives of f_r with respect to p, q and r are written:

$$\nabla_p f_q = \frac{I_t - I_x}{I_t}r - \frac{1}{I_t}\overline{q}Sd\left(\frac{d}{V}\right)C_{np\alpha}(M)\beta, \tag{50}$$

$$\nabla_q f_q = \frac{1}{I_t}\overline{q}Sd\left(\frac{d}{V}\right)C_{mq}(M), \tag{51}$$

$$\nabla_r f_q = \frac{I_t - I_x}{I_t}p. \tag{52}$$

The second term in Equation (50) may be neglected since it is divided by V and the expression can thus be further simplified. Concerning now differentiation with respect to u, v and w, matters are more complicated. Indeed, Equation (24) depends on α_t, which is a function of α, β, and both are also functions of the linear velocities:

$$\alpha = \arctan\frac{w}{u} \quad \text{and} \quad \beta = \arctan\frac{v}{u}. \tag{53}$$

Referring to Equation (24), and comparing once again to numerical linearization, it can be shown that in order to compute $\nabla_u f_q$, derivating the first parenthesis term involving $C_{m\alpha}$ suffices. In addition, only two derivations contribute significantly; those involving $\nabla_u \overline{q}$ and $\nabla_u \alpha$. To compute the derivatives $\nabla_v f_q, \nabla_w f_q$ the terms involving the Magnus moment should be considered also; in addition derivating with respect to $\overline{q}$ can be simplified. Compute first the derivatives concerning $\nabla_u f_q$:

$$\nabla_u \alpha = \frac{-w}{u^2 + w^2} \quad \text{and} \quad \nabla_u \overline{q} = \rho\, u. \tag{54}$$

We obtain thus:

$$\begin{aligned}\nabla_u f_q &= \frac{1}{I_\mathrm{t}}\overline{q}SdC_{\mathrm{m}\alpha}(\alpha_\mathrm{t},M)\nabla_u\alpha + \frac{1}{I_\mathrm{t}}SdC_{\mathrm{m}\alpha}(\alpha_\mathrm{t},M)\alpha\nabla_u\overline{q}\\ &= \frac{1}{I_\mathrm{t}}\overline{q}S\left(\frac{d}{V}\right)C_{\mathrm{m}\alpha}(\alpha_\mathrm{t},M)\left[-\frac{w}{u^2+w^2}V + 2\left(\frac{u}{V}\right)\alpha\right].\end{aligned} \tag{55}$$

To compute $\nabla_v f_q$ and $\nabla_w f_q$, we follow the above method and since:

$$\nabla_v\alpha = \nabla_w\beta = 0, \quad \nabla_w\alpha = \frac{u}{u^2+w^2} \quad \text{and} \quad \nabla_v\beta = \frac{u}{u^2+v^2}, \tag{56}$$

the derivatives $\nabla_v f_q$ and $\nabla_w f_q$ are written as:

$$\nabla_v f_q = -\frac{1}{I_\mathrm{t}}\overline{q}Sd\left(\frac{d}{V}\right)C_{\mathrm{n}p\alpha}(M)\frac{u}{u^2+v^2}p, \tag{57}$$

$$\nabla_w f_q = \frac{1}{I_\mathrm{t}}\overline{q}S\left(\frac{d}{V}\right)C_{\mathrm{m}\alpha}(\alpha_\mathrm{t},M)\frac{u}{u^2+w^2}V. \tag{58}$$

Finally, concerning the derivation with respect to z_e, it can be shown that derivation of Equation (24) only with respect to the air density ρ suffices to obtain correct results. In addition if only the first parenthesis term is considered, then the results remain very accurate and we obtain:

$$\nabla_{z_\mathrm{e}} f_q = \frac{1}{2I_\mathrm{t}}SdV^2C_{\mathrm{m}\alpha}(\alpha_\mathrm{t},M)\alpha\,\nabla_{z_\mathrm{e}}\rho. \tag{59}$$

As an illustrative example we give in Figure (8) the derivative $\nabla_r f_q$; we may see from Equation (52) that it is proportional to p by a factor $\frac{I_\mathrm{t}-I_\mathrm{x}}{I_\mathrm{t}} \simeq 0.92$ and thus very significant in amplitude with respect to the other derivatives due to the projectile's high spin rates.

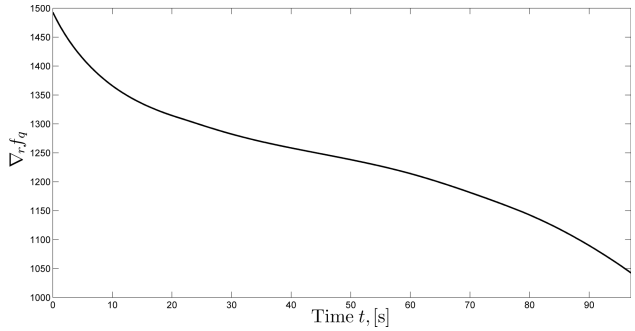

Figure 8. Derivative $\nabla_r f_q$.

3. Yaw Velocity Linearization

The yaw velocity linearization can be carried out in the same fashion as the pitch described in Section III.B.2. Referring to Equation (25), we obtain the following equations:

$$\nabla_p f_r = \frac{I_\mathrm{x}-I_\mathrm{t}}{I_\mathrm{t}}q - \frac{1}{I_\mathrm{t}}\overline{q}Sd\left(\frac{d}{V}\right)C_{\mathrm{n}p\alpha}(M)\alpha, \tag{60}$$

$$\nabla_q f_r = \frac{I_\mathrm{x}-I_\mathrm{t}}{I_\mathrm{t}}p, \tag{61}$$

$$\nabla_r f_r = \frac{1}{I_\mathrm{t}}\overline{q}Sd\left(\frac{d}{V}\right)C_{\mathrm{n}r}(M). \tag{62}$$

The second term's contribution in Equation (60) is small due to the multiplication with α and thus the derivative $\nabla_p f_r$ follows a similar pattern to that of q since $\frac{I_\mathrm{x}-I_\mathrm{t}}{I_\mathrm{t}} \simeq -0.92$.

In regards to the derivation with respect to the linear velocities u, v and w, we follow the same procedure as described in the previous section and obtain:

$$\nabla_u f_r = \frac{1}{I_{\rm t}} \overline{q} S \left(\frac{d}{V}\right) C_{{\rm n}\beta}(\alpha_{\rm t}, M) \left[-\frac{v}{u^2+v^2} V + 2\left(\frac{u}{V}\right)\beta \right], \tag{63}$$

$$\nabla_v f_r = \frac{1}{I_{\rm t}} \overline{q} S \left(\frac{d}{V}\right) C_{{\rm n}\beta}(\alpha_{\rm t}, M) \frac{u}{u^2+v^2} V, \tag{64}$$

$$\nabla_w f_r = -\frac{1}{I_{\rm t}} \overline{q} S d \left(\frac{d}{V}\right) C_{{\rm np}\alpha}(M) \frac{u}{u^2+w^2} p. \tag{65}$$

Finally, similarly to Equation (59) $\nabla_{z_{\rm e}} f_r$ is computed as:

$$\nabla_{z_{\rm e}} f_r = \frac{1}{2I_{\rm t}} S d V^2 C_{{\rm n}\beta}(\alpha_{\rm t}, M) \beta \nabla_{z_{\rm e}} \rho. \tag{66}$$

As an illustrative example we give here the two derivatives $\nabla_u f_r$ and $\nabla_w f_r$; we can see from Figures (9)-(10) that even though these terms are not as large as $\nabla_q f_r$, they nevertheless remain significant and should be taken into account.

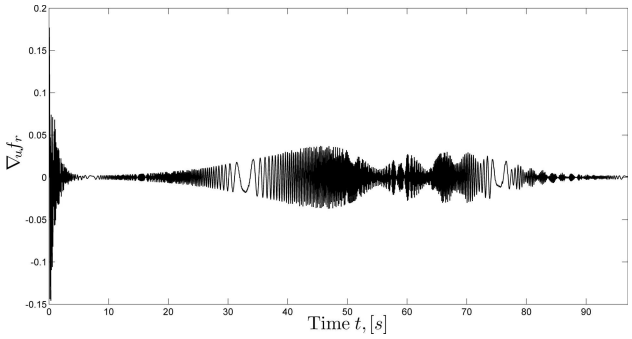

Figure 9. Derivative $\nabla_u f_r$.

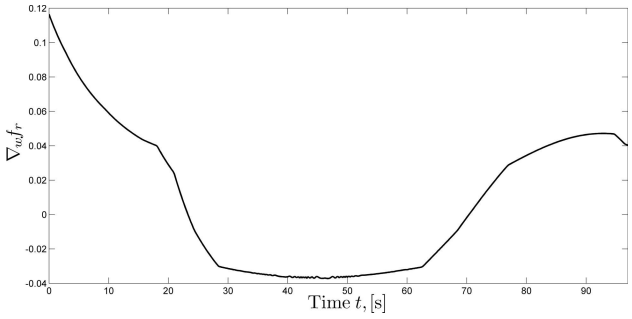

Figure 10. Derivative $\nabla_w f_r$.

4. Longitudinal Velocity Linearization

The force dynamics depend on the Euler angles ϕ and θ also and thus we have some additional derivatives with respect to the moment dynamics. Using Equation (20) we obtain:

$$\nabla_q f_u = -w, \tag{67}$$

$$\nabla_r f_u = v, \tag{68}$$

$$\nabla_\theta f_u = -g c_\theta. \tag{69}$$

Derivating with respect to the linear velocities is similar to the analysis of Section III.B.1. Rewrite Equation (20) as $f_u = rv - qw - gs_\theta - \frac{1}{2m}\rho S C_{\rm A}(\alpha_{\rm t}, M) V^2$, where we have isolated terms depending on the linear velocities. Numerical techniques show that derivation with respect to $\alpha_{\rm t}$ is redundant and:

$$\nabla_u \Big[C_{\rm A}(\alpha_{\rm t}, M) V^2 \Big] = 2u C_{\rm A}(\alpha_{\rm t}, M) + uM \nabla_M C_{\rm A}(\alpha_{\rm t}, M). \tag{70}$$

Using Equation (70), the derivatives $\nabla_u f_u, \nabla_u f_v$ and $\nabla_u f_w$ can be written:

$$\nabla_u f_u = -\frac{1}{m}\overline{q}S\frac{u}{V^2}\Big[2C_A + M\nabla_M C_{\mathrm{A}}(\alpha_{\mathrm{t}}, M)\Big], \tag{71}$$

$$\nabla_v f_u = r - \frac{1}{m}\overline{q}S\frac{v}{V^2}\Big[2C_A + M\nabla_M C_{\mathrm{A}}(\alpha_{\mathrm{t}}, M)\Big], \tag{72}$$

$$\nabla_w f_u = -q - \frac{1}{m}\overline{q}S\frac{w}{V^2}\Big[2C_A + M\nabla_M C_{\mathrm{A}}(\alpha_{\mathrm{t}}, M)\Big]. \tag{73}$$

Note that the second term in the parenthesis in Equations (72)-(73) may be also neglected. Finally, the element $\nabla_{z_{\mathrm{e}}} f_u$ is computed by only derivating with respect to the air density (see also Figure (11)):

$$\nabla_{z_{\mathrm{e}}} f_u = -\frac{1}{2m}SV^2 C_{\mathrm{A}}(\alpha_{\mathrm{t}}, M)\nabla_{z_{\mathrm{e}}}\rho. \tag{74}$$

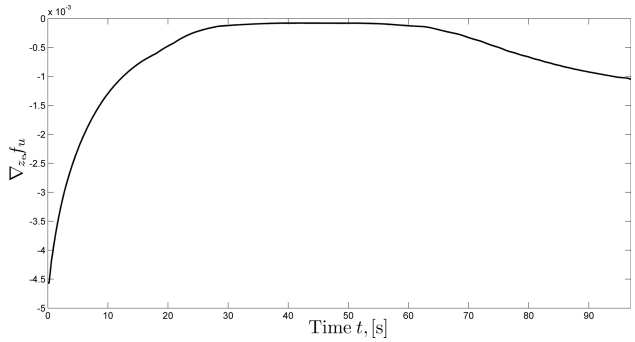

Figure 11. Derivative $\nabla_{z_{\mathrm{e}}} f_u$.

5. Lateral Velocity Linearization

For the lateral velocity linearization, the non-zero derivatives for the angular rates and Euler angles are calculated using Equation (21) as:

$$\nabla_p f_v = w - \frac{1}{m}\overline{q}S\left(\frac{d}{V}\right)C_{yp\alpha}(M)\alpha, \tag{75}$$

$$\nabla_r f_v = -u, \tag{76}$$

$$\nabla_\phi f_v = g c_\phi c_\theta, \tag{77}$$

$$\nabla_\theta f_v = -g s_\phi s_\theta. \tag{78}$$

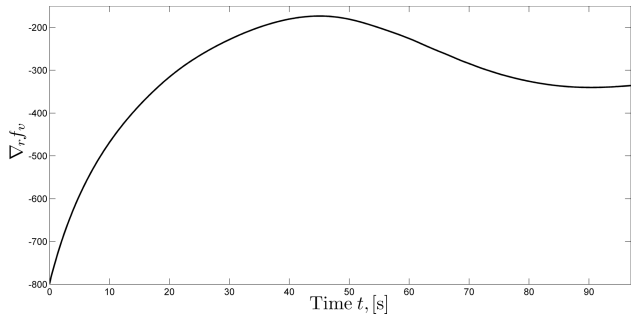

Figure 12. Derivative $\nabla_r f_v$.

Figure (12) shows that the derivative $\nabla_r f_v$ is the most significant in amplitude, since it is equal to the negative of the longitudinal velocity; in addition, the second term in Equation (75) may be neglected.

Concerning now the derivatives with respect to the linear velocities, it has been found that derivating Equation (21) only with respect to α, β provides sufficient accuracy and hence using Equation (54) we obtain:

$$\begin{aligned}\nabla_u f_v &= -r + \frac{1}{m}\overline{q}S\left[C_{\mathrm{Y}\beta}(\alpha_{\mathrm{t}}, M)\nabla_u\beta - \left(\frac{d}{V}\right)C_{yp\alpha}(M)\nabla_u\alpha\, p\right] \\ &= -r + \frac{1}{m}\overline{q}S\left[-C_{\mathrm{Y}\beta}(\alpha_{\mathrm{t}}, M)\frac{v}{u^2+v^2} + \left(\frac{d}{V}\right)C_{yp\alpha}(M)\frac{w}{u^2+w^2}p\right].\end{aligned} \tag{79}$$

The remaining derivatives are calculated in a similar fashion, leading to:

$$\nabla_v f_v = \frac{1}{m}\overline{q}SC_{\mathrm{Y}\beta}(\alpha_{\mathrm{t}}, M)\frac{u}{u^2+v^2}, \tag{80}$$

$$\nabla_w f_v = p - \frac{1}{m}\overline{q}S\left(\frac{d}{V}\right)C_{yp\alpha}(M)\frac{u}{u^2+w^2}p. \tag{81}$$

Neglecting the influence of the speed of sound and of the Magnus force aerodynamic function, the derivative $\nabla_{z_{\mathrm{e}}} f_v$ is calculated as:

$$\nabla_{z_{\mathrm{e}}} f_v = \frac{1}{2m}SV^2C_{\mathrm{Y}\beta}(\alpha_{\mathrm{t}}, M)\beta\,\nabla_{z_{\mathrm{e}}}\rho. \tag{82}$$

6. Normal Velocity Linearization

To calculate the normal velocity derivatives, we proceed in the same fashion as was described in Section III.B.5 for the lateral velocity. The non-zero elements are:

$$\nabla_p f_w = -v + \frac{1}{m}\overline{q}S\left(\frac{d}{V}\right)C_{yp\alpha}(M)\beta, \tag{83}$$

$$\nabla_q f_w = u, \tag{84}$$

$$\nabla_\phi f_w = -gs_\phi c_\theta, \tag{85}$$

$$\nabla_\theta f_w = -gc_\phi s_\theta, \tag{86}$$

$$\nabla_u f_w = q - \frac{1}{m}\overline{q}S\left[C_{\mathrm{N}\alpha}(\alpha_{\mathrm{t}}, M)\frac{w}{u^2+w^2} + \left(\frac{d}{V}\right)C_{yp\alpha}(M)\frac{v}{u^2+v^2}p\right], \tag{87}$$

$$\nabla_v f_w = -p + \frac{1}{m}\overline{q}S\left(\frac{d}{V}\right)C_{yp\alpha}(M)\frac{u}{u^2+v^2}p, \tag{88}$$

$$\nabla_w f_w = \frac{1}{m}\overline{q}SC_{\mathrm{N}\alpha}(\alpha_{\mathrm{t}}, M)\frac{w}{u^2+w^2}, \tag{89}$$

$$\nabla_{z_{\mathrm{e}}} f_w = \frac{1}{2m}SV^2C_{\mathrm{N}\alpha}(\alpha_{\mathrm{t}}, M)\alpha\,\nabla_{z_{\mathrm{e}}}\rho. \tag{90}$$

The second term in Equation (83) may be neglected, whereas for Equation (90), derivating only with respect to the air density again suffices. As an illustration we represent $\nabla_w f_w$ in Figure (13).

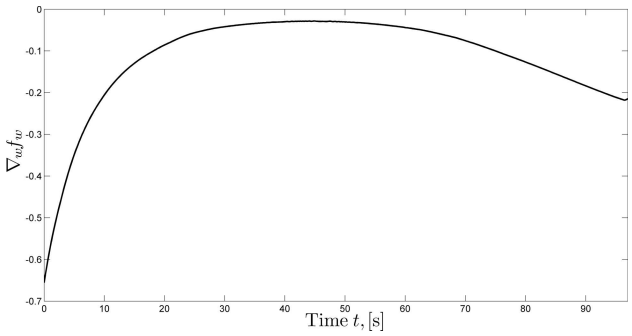

Figure 13. Derivative $\nabla_w f_w$.

IV. LTV Model Structure

In Section III.B we have seen that the linear time-varying projectile dynamics $\mathscr{S}_{x_\mathrm{d}}$ along the trajectory are written in the following way:

$$\mathscr{S}_{\mathbf{x}_\mathrm{d}}: \quad \dot{\mathbf{x}}_{\mathrm{d}\delta} = \mathbf{A}_{\mathrm{dd}}(t)\mathbf{x}_{\mathrm{d}\delta} + \mathbf{w}, \tag{91}$$

where $\mathbf{w} = \mathbf{A}_{\mathrm{dk}}(t)\mathbf{x}_{\mathrm{k}\delta}$. The state (or else stability) matrix $\mathbf{A}_{\mathrm{dd}}$ and the perturbation matrix $\mathbf{A}_{\mathrm{dk}}$ may be further decomposed as:

$$\mathbf{A}_{\mathrm{dd}} = \left[\begin{array}{c|c} \mathbf{A}_{\boldsymbol{\omega\omega}} & \mathbf{A}_{\boldsymbol{\omega v}} \\ \hline \mathbf{A}_{\mathbf{v}\boldsymbol{\omega}} & \mathbf{A}_{\mathbf{vv}} \end{array}\right], \tag{92}$$

$$\mathbf{A}_{\mathrm{dk}} = \left[\begin{array}{c|c} \mathbf{A}_{\boldsymbol{\omega e}} & \mathbf{A}_{\boldsymbol{\omega s}} \\ \hline \mathbf{A}_{\mathbf{ve}} & \mathbf{A}_{\mathbf{vs}} \end{array}\right]. \tag{93}$$

Regrouping the results of Sections III.B.1-III.B.6, the matrices forming the stability matrix are presented in Equations (98)-(101) in the following page whereas the matrices forming the perturbation matrix are:

$$\mathbf{A}_{\boldsymbol{\omega e}} = \mathbb{O}_{3\times 3}, \tag{94}$$

$$\mathbf{A}_{\boldsymbol{\omega s}} = \begin{bmatrix} 0 & 0 & \dfrac{1}{2I_\mathrm{x}} SdV^2 \left(\dfrac{d}{V}\right) C_{\mathrm{l}p}(M)\nabla_{z_\mathrm{e}}\rho\, p \\ 0 & 0 & \dfrac{1}{2I_\mathrm{t}} SdV^2 C_{\mathrm{m}\alpha}(\alpha_\mathrm{t}, M)\alpha\, \nabla_{z_\mathrm{e}}\rho \\ 0 & 0 & \dfrac{1}{2I_\mathrm{t}} SdV^2 C_{\mathrm{n}\beta}(\alpha_\mathrm{t}, M)\beta\, \nabla_{z_\mathrm{e}}\rho \end{bmatrix}, \tag{95}$$

$$\mathbf{A}_{\mathbf{ve}} = \begin{bmatrix} 0 & -gc_\theta & 0 \\ gc_\phi c_\theta & -gs_\phi s_\theta & 0 \\ -gs_\phi c_\theta & -gc_\phi s_\theta & 0 \end{bmatrix}, \tag{96}$$

$$\mathbf{A}_{\mathbf{vs}} = \begin{bmatrix} 0 & 0 & -\dfrac{1}{2m} SV^2 C_\mathrm{A}(\alpha_\mathrm{t}, M)\nabla_{z_\mathrm{e}}\rho \\ 0 & 0 & \dfrac{1}{2m} SV^2 C_{\mathrm{Y}\beta}(\alpha_\mathrm{t}, M)\beta\, \nabla_{z_\mathrm{e}}\rho \\ 0 & 0 & \dfrac{1}{2m} SV^2 C_{\mathrm{N}\alpha}(\alpha_\mathrm{t}, M)\alpha\, \nabla_{z_\mathrm{e}}\rho \end{bmatrix}. \tag{97}$$

Starting from the perturbation matrices describing the kinematics' states influence on the dynamics states appearing in Equations (94)-(97), we notice that $\mathbf{A}_{\boldsymbol{\omega e}}$ is zero, since the moment dynamics do not depend on the Euler angles but only on the altitude z_e. This is the reason why the first two columns of $\mathbf{A}_{\boldsymbol{\omega s}}$ are also zero. The matrix $\mathbf{A}_{\mathbf{ve}}$ represents the influence of the Euler angles on the linear velocities; we clearly see that the yaw angle column is empty as expected. Finally concerning $\mathbf{A}_{\mathbf{vs}}$, we note that there is no influence of the longitudinal or normal position on the linear velocity vector, while the altitude component still remains.

Concerning now the stability matrices appearing in Equations (98)-(101), we may remark that they are full of dependencies and there is only a small number of zero components. The matrix $\mathbf{A}_{\boldsymbol{\omega\omega}}$ contains components that are small-medium in amplitude, except for the ones that are proportional to the projectile rotational velocity p being large for stability reasons. Relatively small but still important dependencies are also present in matrix $\mathbf{A}_{\boldsymbol{\omega v}}$. Regarding the linear velocity matrices, we may note that the components of matrix $\mathbf{A}_{\mathbf{v}\boldsymbol{\omega}}$ are rather large due to the important values of the linear velocity vector affecting it. Similarly, matrix $\mathbf{A}_{\mathbf{vv}}$ also features some large terms because of the fact that they are directly proportional to the roll velocity.

As a final comment it can be pointed out that there exists a significant number of matrix elements computed in Section III demonstrating rapid oscillations as for example $\nabla_u f_r$ illustrated in Figure (9); however due to space restrictions not every matrix element has been depicted in this paper. The reason for these oscillations is clearly the body-rolling frame turning with the projectile; as a consequence the time trajectory of a number of states (q, r, v and w in particular) is modulated by the rolling velocity p. Given the fact that the linearization matrices presented in Equation (91) are evaluated along the state reference trajectory $\mathcal{T}_\mathrm{r}$, this explains the reason why these elements demonstrate such a behavior. Comparison studies are currently investigated for the case of a non-rolling body frame.

$$\mathbf{A}_{\boldsymbol{\omega}\boldsymbol{\omega}} = \begin{bmatrix} \frac{1}{I_{\mathrm{x}}}\overline{q}Sd\left(\frac{d}{V}\right)C_{\mathrm{l}p}(M) & 0 & 0 \\ \frac{I_{\mathrm{t}}-I_{\mathrm{x}}}{I_{\mathrm{t}}}r - \frac{1}{I_{\mathrm{t}}}\overline{q}Sd\left(\frac{d}{V}\right)C_{\mathrm{n}p\alpha}(M)\beta & \frac{1}{I_{\mathrm{t}}}\overline{q}Sd\left(\frac{d}{V}\right)C_{\mathrm{m}q}(M) & \frac{I_{\mathrm{t}}-I_{\mathrm{x}}}{I_{\mathrm{t}}}p \\ \frac{I_{\mathrm{x}}-I_{\mathrm{t}}}{I_{\mathrm{t}}}q - \frac{1}{I_{\mathrm{t}}}\overline{q}Sd\left(\frac{d}{V}\right)C_{\mathrm{n}p\alpha}(M)\alpha & \frac{I_{\mathrm{x}}-I_{\mathrm{t}}}{I_{\mathrm{t}}}p & \frac{1}{I_{\mathrm{t}}}\overline{q}Sd\left(\frac{d}{V}\right)C_{\mathrm{n}r}(M) \end{bmatrix} \tag{98}$$

$$\mathbf{A}_{\boldsymbol{\omega}\mathbf{v}} = \begin{bmatrix} \frac{1}{I_{\mathrm{x}}}\overline{q}Sd\left(\frac{d}{V}\right)\frac{u}{V^2}\Big[C_{\mathrm{l}p}(M) + M\nabla_M C_{\mathrm{l}p}(M)\Big]p & \frac{1}{I_{\mathrm{x}}}\overline{q}Sd\left(\frac{d}{V}\right)\frac{v}{V^2}C_{\mathrm{l}p}(M)p & \frac{1}{I_{\mathrm{x}}}\overline{q}Sd\left(\frac{d}{V}\right)\frac{w}{V^2}C_{\mathrm{l}p}(M)p \\ \frac{1}{I_{\mathrm{t}}}\overline{q}S\left(\frac{d}{V}\right)C_{\mathrm{m}\alpha}(\alpha_{\mathrm{t}},M)\left[-\frac{w}{u^2+w^2}V + 2\left(\frac{u}{V}\right)\alpha\right] & -\frac{1}{I_{\mathrm{t}}}\overline{q}Sd\left(\frac{d}{V}\right)C_{\mathrm{n}p\alpha}(M)\frac{u}{u^2+v^2}p & \frac{1}{I_{\mathrm{t}}}\overline{q}S\left(\frac{d}{V}\right)C_{\mathrm{m}\alpha}(\alpha_{\mathrm{t}},M)\frac{u}{u^2+w^2}V \\ \frac{1}{I_{\mathrm{t}}}\overline{q}S\left(\frac{d}{V}\right)C_{\mathrm{n}\beta}(\alpha_{\mathrm{t}},M)\left[-\frac{v}{u^2+v^2}V + 2\left(\frac{u}{V}\right)\beta\right] & \frac{1}{I_{\mathrm{t}}}\overline{q}S\left(\frac{d}{V}\right)C_{\mathrm{n}\beta}(\alpha_{\mathrm{t}},M)\frac{u}{u^2+v^2}V & -\frac{1}{I_{\mathrm{t}}}\overline{q}Sd\left(\frac{d}{V}\right)C_{\mathrm{n}p\alpha}(M)\frac{u}{u^2+w^2}p \end{bmatrix} \tag{99}$$

$$\mathbf{A}_{\mathbf{v}\boldsymbol{\omega}} = \begin{bmatrix} 0 & -w & v \\ w - \frac{1}{m}\overline{q}S\left(\frac{d}{V}\right)C_{\mathrm{y}p\alpha}(M)\alpha & 0 & -u \\ -v + \frac{1}{m}\overline{q}S\left(\frac{d}{V}\right)C_{\mathrm{y}p\alpha}(M)\beta & u & 0 \end{bmatrix} \tag{100}$$

$$\mathbf{A}_{\mathbf{v}\mathbf{v}} = \begin{bmatrix} -\frac{1}{m}\overline{q}S\frac{u}{V^2}\Big[2C_A(\alpha_{\mathrm{t}},M) + M\nabla_M C_{\mathrm{A}}(\alpha_{\mathrm{t}},M)\Big] & r - \frac{2}{m}\overline{q}S\frac{v}{V^2}C_A(\alpha_{\mathrm{t}},M) & -q - \frac{2}{m}\overline{q}S\frac{w}{V^2}C_A(\alpha_{\mathrm{t}},M) \\ -r + \frac{1}{m}\overline{q}S\left[-C_{\mathrm{Y}\beta}(\alpha_{\mathrm{t}},M)\frac{v}{u^2+v^2} + \left(\frac{d}{V}\right)C_{\mathrm{y}p\alpha}(M)\frac{w}{u^2+w^2}p\right] & \frac{1}{m}\overline{q}SC_{\mathrm{Y}\beta}(\alpha_{\mathrm{t}},M)\frac{u}{u^2+v^2} & p - \frac{1}{m}\overline{q}S\left(\frac{d}{V}\right)C_{\mathrm{y}p\alpha}(M)\frac{u}{u^2+w^2}p \\ q + \frac{1}{m}\overline{q}S\left[-C_{\mathrm{N}\alpha}(\alpha_{\mathrm{t}},M)\frac{w}{u^2+w^2} - \left(\frac{d}{V}\right)C_{\mathrm{y}p\alpha}(M)\frac{v}{u^2+v^2}p\right] & -p + \frac{1}{m}\overline{q}S\left(\frac{d}{V}\right)C_{\mathrm{y}p\alpha}(M)\frac{u}{u^2+v^2}p & \frac{1}{m}\overline{q}SC_{\mathrm{N}\alpha}(\alpha_{\mathrm{t}},M)\frac{u}{u^2+w^2} \end{bmatrix} \tag{101}$$

V. Stability Analysis

The previous sections described the derivation of a LTV model $\mathscr{S}_{\mathbf{x}_\mathrm{d}}$ of the projectile dynamics along the reference trajectory $\mathcal{T}_\mathrm{r}$. The model form presented in Equation (91) involves the stability matrix $\mathbf{A}_\mathrm{dd}(t)$, affecting the projectile's internal stability, along with an external perturbation $\mathbf{w}$. The stability properties of the projectile's dynamics can be studied by assessing the stability of the origin $\mathbf{x}_{\mathrm{d}\delta} = 0$ of this system perturbed by the exogenous signal $\mathbf{w}$. An early theorem for forced LTV systems exists and characterizes the boundedness of the state trajectory when the state dynamics are perturbed by an external signal.[5] It states, in brief, that if the state transition matrix of the LTV system is continuous, has decaying properties, and the external perturbation is bounded, then the state trajectory also remains bounded. The problem then consists in studying the stability properties of an unforced LTV system of the general form $\dot{\mathbf{x}} = \mathbf{A}(t)\mathbf{x}$; this task is not trivial and a large literature exists on the issue.[6,12,20]

The condition that a matrix $\mathbf{A}(\tau), \forall \tau = t \geq t_0$ be Hurwitz (i.e. $\lambda_i\{\mathbf{A}(\tau)\} \in \overline{\mathscr{C}}_-, i = 1, \ldots, n$), often considered in practice, does not suffice theoretically since it is neither a necessary nor a sufficient condition for stability. This type of frozen-time analysis is though preferred in real-life situations since it yields quick results by only studying the system eigenvalues. A slowness condition involving the time variation of $\mathbf{A}(t)$ must be also added ($\mathbf{A}(t)$ should also have bounded elements) to complete the stability analysis. The purpose of this work is not to focus on theoretically proving the stability or instability of the projectile, hence we will restrict ourselves to a more quantitative analysis by computing the matrix $\mathbf{A}_\mathrm{dd}(t)$ eigenvalues along the projectile flight path and compare with classic aeroballistic stability analysis.

A. Frozen-time eigenvalue stability analysis

The eigenvalues of the stability matrix $\mathbf{A}_\mathrm{dd}(t)$ for the given initial conditions and a total flight time $\Delta t_\mathrm{f} = 97\mathrm{s}$ are shown in Figure (14). We note that there exist two pairs of complex conjugate eigenvalues $\lambda_{2,3}, \lambda_{5,6}$ and two real ones λ_1, λ_4. Both $\lambda_{2,3}$ and λ_1, λ_4 are always stable, but the second pair $\lambda_{5,6}$ is not. The resulting unstable flight phase Δt_un, which represents the 40% of the total flight time, is:

$$\Delta t_\mathrm{un} : \ 26.6\mathrm{s} \leq t \leq 65.0\mathrm{s}. \tag{102}$$

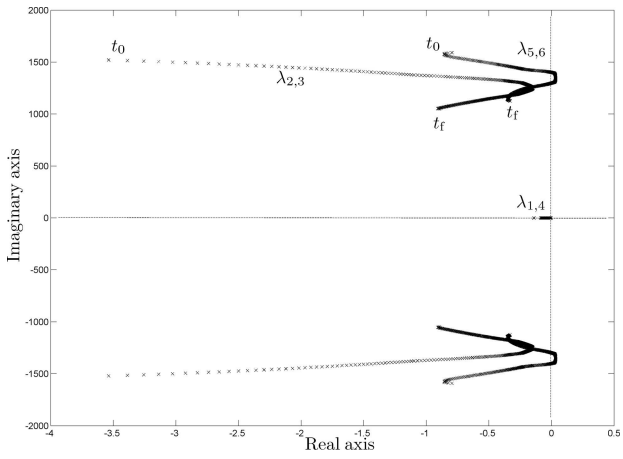

Figure 14. Stability matrix eigenvalues.

The system modes corresponding to the angular velocities may be computed with significant precision directly from the matrix $\mathbf{A}_{\boldsymbol{\omega}\boldsymbol{\omega}}$. Given the aerodynamic function symmetry $C_{\mathrm{m}q} = C_{\mathrm{n}r}$ we obtain:

$$\lambda_1 \simeq \frac{1}{I_\mathrm{x}} \overline{q} S d \left(\frac{d}{V}\right) C_{\mathrm{l}p}(M), \tag{103}$$

$$\lambda_{2,3} \simeq \frac{1}{I_\mathrm{t}} \overline{q} S d \left(\frac{d}{V}\right) C_{\mathrm{m}q}(M) \pm \frac{I_\mathrm{t} - I_\mathrm{x}}{I_\mathrm{t}} p \jmath. \tag{104}$$

Since $C_{\mathrm{l}p}(M), C_{\mathrm{m}q}(M) < 0$, these eigenvalues correspond to stable modes and the significant imaginary parts are explained by the large roll velocity values. Figure (15) shows the modes calculated using both matrices $\mathbf{A}_\mathrm{dd}(t)$ and $\mathbf{A}_{\boldsymbol{\omega}\boldsymbol{\omega}}(t)$; we verify that the results are very close.

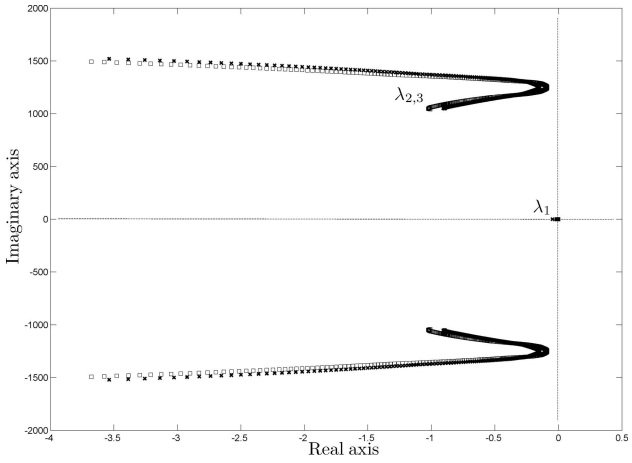

Figure 15. Angular velocity modes.

Since matrix $\mathbf{A_{\omega v}}$ is not zero, it is not possible to compute $\lambda_{5,6}$, determining the projectile stability, using only matrix $\mathbf{A_{vv}}$. However, if all the elements of matrix $\mathbf{A_{\omega v}}$ are set to zero except for the terms $\mathbf{A_{\omega v}}(2,5), \mathbf{A_{\omega v}}(3,6)$, the real parts of eigenvalues $\lambda_{5,6}$, affecting stability, are not significantly altered during the instability timespan. Figure (16) shows a comparison when computing $\Re\{\lambda_{5,6}(t)\}$ using the above procedure. It has been numerically verified that when the eigenvalues are unstable these two terms are negative; conversely the instability timespan can be estimated by computing the time period for which $\mathbf{A_{\omega v}}(2,5), \mathbf{A_{\omega v}}(3,6) > 0$. Referring to Equations (57), (65), we may see that this condition is surprisingly simple, being in fact a sign condition on the Magnus moment aerodynamic coefficient:

$$C_{np\alpha}\big(M(t)\big) > 0. \tag{105}$$

This condition results to an approximated instability region given by:

$$\hat{\Delta} t_{\text{un}} : \ 23.3\text{s} \leq t \leq 70.3\text{s}. \tag{106}$$

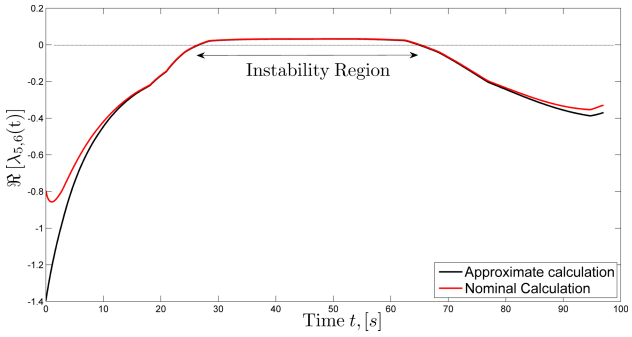

Figure 16. Real part eigenvalue computation comparison.

B. Aeroballistic stability analysis

Classic aeroballistic theory[18] states that the projectile is stable when the conditions:

$$S_{\text{g}} > 1 \quad \text{and} \quad \frac{1}{S_{\text{g}}} < S_{\text{d}}(2 - S_{\text{d}}) \tag{107}$$

are satisfied. The gyroscopic and dynamic stability coefficients involved in these two conditions are defined as:

$$S_{\text{g}} = \frac{P_{\text{g}}^2}{4M_{\text{g}}} \quad \text{and} \quad S_{\text{d}} = \frac{2T_{\text{d}}}{H_{\text{d}}}. \tag{108}$$

The factors entering Equation (108) are defined as (our definition for $C_{\mathrm{np}\alpha}$ is different from the one employed in Ref. 18 and hence a minus sign is needed in Equation (111)):

$$P_{\mathrm{g}} = \frac{I_{\mathrm{x}}}{I_{\mathrm{t}}}\frac{d}{V}p, \tag{109}$$

$$M_{\mathrm{g}} = \frac{md^2}{I_{\mathrm{t}}}\frac{\rho Sd}{2m}C_{\mathrm{m}\alpha}(\alpha_{\mathrm{t}}, M), \tag{110}$$

$$T_{\mathrm{d}} = \frac{\rho Sd}{2m}\left[C_{\mathrm{L}\alpha}(\alpha_{\mathrm{t}}, M) - \frac{md^2}{I_{\mathrm{x}}}C_{\mathrm{np}\alpha}(M)\right], \tag{111}$$

$$H_{\mathrm{d}} = \frac{\rho Sd}{2m}\left[C_{\mathrm{L}\alpha}(\alpha_{\mathrm{t}}, M) - C_{\mathrm{D}\alpha}(\alpha_{\mathrm{t}}, M) - \frac{md^2}{I_{\mathrm{t}}}C_{\mathrm{mq}}(M)\right]. \tag{112}$$

Evaluating the conditions of Equation (107) along the projectile trajectory we verify that the first involving S_{g} always holds. It is the second condition that permits us to calculate an approximation of the unstable flight phase $\hat{\Delta}t^*_{\mathrm{un}}$ is illustrated in Figure (17). Hence by inspection we obtain:

$$\hat{\Delta}t^*_{\mathrm{un}} : \ 26.0\mathrm{s} \leq t \leq 65.7\mathrm{s}. \tag{113}$$

An alternative visualization, familiar mostly to aeroballistic experts is given in Figure (18), where $\frac{1}{S_{\mathrm{g}}}$ is plotted versus S_{d}. The red line draws the right hand of Equation's (107) second condition and corresponds to the limit between the stable and unstable portions of the projectile trajectory.

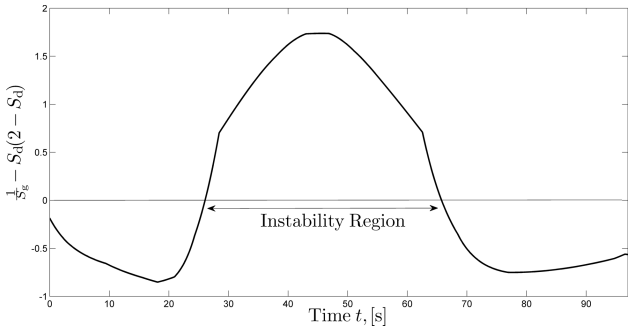

Figure 17. Aeroballistic theory stability condition.

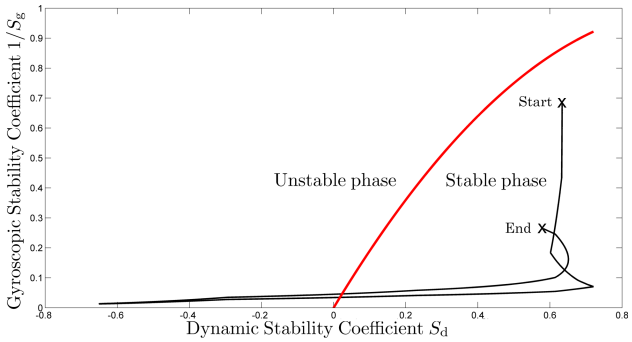

Figure 18. Aeroballistic theory stability diagram.

In this section we have provided a comparison of three alternative methods for assessing the projectile's stability properties; the first uses frozen-time eigenvalue analysis theory, the second an heuristic condition on the Magnus moment coefficient whereas the third is based on classic approximative aeroballistic theory results. The first method provides results that are almost identical to the ones provided by the third method; the former should also be the most accurate because it involves no approximations since it computes directly the system eigenvalues. Another advantage is that it proposes a way of analyzing stability of any projectile concept (with control surfaces or not and with various levels of refinement for the aerodynamic coefficients). The second method provides a less accurate but very simple condition for stability; its validity remains however to be verified for other flight conditions and configurations.

VI. Conclusions

In this paper a nonlinear modeling of the 155mm spinning projectile dynamics without control surfaces was detailed using a tensor formulation. An accurate LTV mathematical model of the nonlinear dynamics was then derived using a trajectory-based linearization technique and has been validated using numerical linearization tools. The model structure was discussed and the various state-space matrices were given. A comprehensive stability analysis of the projectile trajectory was finally performed using this LTV model and was compared to existing approximative aeroballistic theory results. Finally an heuristic condition, allowing to obtain an approximation of the unstable flight phase, valid for the flight conditions studied was proposed.

References

[1]I.-J. Adounkpé. *Robustesse dans un Cadre Non-Linéaire : Application au Pilotage des Missiles*. PhD thesis, Université Paris-Sud XI/SUPELEC, France, 2004.

[2]B. Burchett and M. Costello. Model Predictive Lateral Pulse Jet Control of an Atmospheric Rocket. *Journal of Guidance, Control and Dynamics*, 25(5):860–867, 2002.

[3]M. Costello and R. Agarwalla. Improved Dispersion of a Fin-Stabilized Projectile Using a Passive Movable Nose. *Journal of Guidance, Control and Dynamics*, 23(5):900–903, 2000.

[4]M. Costello and A. Peterson. Linear Theory of a Dual-Spin Projectile in Atmospheric Flight. *Journal of Guidance, Control and Dynamics*, 23(5):789–797, 2000.

[5]H. D'Angelo. *Linear Time-Varying Systems: Analysis and Synthesis*. Allyn and Bacon, 1970.

[6]C.A. Desoer. Slowly Varying System $\dot{x} = \mathbf{A}(t)x$. *IEEE Transactions on Automatic Control*, 14(6):780–781, 1969.

[7]C.A. Desoer and M. Vidyasagar. *Feedback Systems: Input-Output Properties*. SIAM, 2009.

[8]C.A. Desoer and K.K. Wong. Small-Signal Behavior of Nonlinear Lumped Networks. *Proceedings of the IEEE*, 56(1):14–22, 1968.

[9]V. Fleck and C. Berner. Increase of Range for an Artillery Projectile by Using the Lift Force. In *Proceedings of the 16th International Symposium on Ballistics*, San Francisco, USA, 1996.

[10]P. Gnemmi and C. Rey. Plasma Actuation for the Control of a Supersonic Projectile. In *Proceedings of the AIAA Guidance, Navigation and Control Conference and Exhibit*, Honolulu, USA, 2008. AIAA.

[11]L. Hainz and M. Costello. Modified Projectile Linear Theory for Rapid Trajectory Prediction. *Journal of Guidance, Control and Dynamics*, 28(5):1006–1014, 2005.

[12]A. Ilchmann, D.H. Owens, and D. Pratzel-Wolters. Sufficient Conditions for Stability of Linear Time-varying Systems. *Systems & Control Letters*, 9, 1987.

[13]M.D. Ilg. *Guidance, Navigation and Control for Munitions*. PhD thesis, Drexel University, USA, 2008.

[14]H. Khalil. *Nonlinear Systems*. Prentice Hall, 2000.

[15]N.A. Lehtomaki. Control of a Spinning Projectile. In *Proceedings of the 4th Meeting of the Coordinating Group on Modern Control Theory*, Rochester, USA, 1982.

[16]D.J. Leith and W.E. Leithead. Survey of Gain Scheduling Analysis and Design. *International Journal of Control*, 73(11):1001–1025, 2000.

[17]K.H. Lloyd and D.P. Brown. Instability of Spinning Projectiles During Terminal Guidance. *Journal of Guidance, Control and Dynamics*, 2, 1979.

[18]R.L. McCoy. *Modern Exterior Ballistics*. Schiffer Publishing Ltd., 1999.

[19]M.C. Mickle and J.J. Zhu. Skid to Turn Control of the APKWS Missile Using Trajectory Linearization Technique. In *Proceedings of the 20th American Control Conference*, Arlington, USA, 2001. IEEE.

[20]H.H. Rosenbrock. The Stability of Linear Time-dependent Control Systems. *International Journal of Electronics and Control*, 15, 1962.

[21]B. Semerci, O. Merttopcuoglu, and O. Tekinalp. Modeling and Robust Control of a Spinning Missile. In *Proceedings of the 22nd IASTED International Conference on Modelling, Identification and Control*, Innsbruck, Austria, 2003.

[22]N. Slegers. Model Predictive Control of a Low Speed Munition. In *Proceedings of the AIAA Atmospheric Flight Conference and Exhibit*, Hilton Head, USA, 2007. AIAA.

[23]S. Theodoulis. *Robust Control in a Nonlinear Context for Large Operating Domains*. PhD thesis, Université Paris-Sud XI/SUPELEC, France, 2008.

[24]M. Vidyasagar. *Nonlinear Systems Analysis*. SIAM, 1993.

[25]P.H. Zipfel. *Modeling and Simulation of Aerospace Vehicle Dynamics*. AIAA Education Series, 2007.